Chemical versus physical grafting of photoluminescent amino-functional carbon dots onto transparent nematic nanocellulose gels and aerogels

Sakeena Quraishi · Sven F. Plappert · Thomas Grießer · Wolfgang Gindl-Altmutter · Falk W. Liebner

Abstract Transparent matrices of low refractive index are promising carriers for photoluminescent nanoparticles targeting true volumetric 3D display applications. Complementation of transparency with a highly open-porous nanomorphology renders respective hybrid gels and aerogels additionally attractive for liquid and gas detection devices. Herein, we present virtually fully bio-based hybrids obtained by decorating highly transparent, nematically ordered gels and aerogels (15–20 mg cm^{-3}) from carboxylated and individualized cellulose nanofibers (i-CNF) with amino-functional photoluminescent carbon dots (CD). The latter were obtained by microwave-assisted hydrothermolysis of lemon juice. As the way of anchoring the CDs onto the large internal surface of the porous i-CNF scaffolds (320 m^2 g^{-1}) has a great impact on the final properties of the hybrid materials including leaching of CDs and reusability of the hybrid, this study assessed the respective pros and cons of a physical and chemical bonding approach. The results confirmed the superiority of covalent grafting. Aqueous carbodiimide coupling of amino-functionalized CDs afforded higher yields of CDs in the final hybrid aerogels, distinctly higher specific surface values (491 m^2 g^{-1}) and slightly enhanced mechanical properties while the high light transmittance and nanomorphology of the i-CNF precursor alcogels is virtually not compromised. Therefore, we conclude that the luminescent i-CNF/CD-chem hybrid materials of this study are promising candidates for environmentally friendly chemical sensing and volumetric display applications.

Sakeena Quraishi and Sven F. Plappert contributed equally to this work.

S. Quraishi · S. F. Plappert · F. W. Liebner (✉)
Division of Chemistry of Renewable Resources, University of Natural Resources and Life Sciences Vienna, Konrad-Lorenz-Straße 24, 3430 Tulln, Austria
e-mail: falk.liebner@boku.ac.at

S. F. Plappert
ICCF, SIGMA Clermont, 63000 Clermont-Ferrand, France

T. Grießer
Chair of Chemistry of Polymeric Materials, University of Leoben, Otto Glöckel-Straße 2/IV, 8700 Leoben, Austria

W. Gindl-Altmutter
Institute of Wood Technology and Renewable, University of Natural Resources and Life Sciences Vienna, Konrad-Lorenz-Straße 24, 3430 Tulln, Austria

Graphic abstract
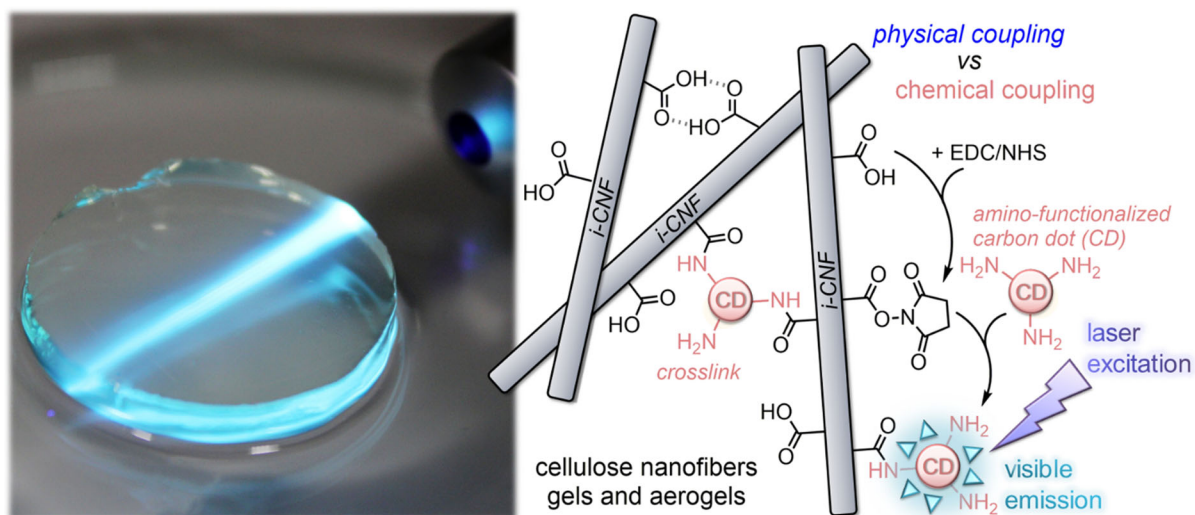
Introduction

Self-assembly (Jiang and Hsieh 2016; Kobayashi et al. 2014; Saito et al. 2011) of individualized cellulosic nanofibers (*i*-CNF) in aqueous colloidal dispersion state is an interesting phenomenon. It is currently intensively explored since it gives access to a new family of fully bio-based free-standing gels (Saito et al. 2011) and aerogels (Kobayashi et al. 2014) that feature intriguing properties. Anisotropic *i*-CNF aerogels have been demonstrated to bear a great potential for high-performance thermal insulation (Kobayashi et al. 2014; Plappert et al. 2017), nanoparticle filtration (Toivonen et al. 2015), or as templates for nanostructuration (Korhonen et al. 2011; Li and Huang 2016; Olsson et al. 2010; Zhu et al. 2018). Their large specific surface, high light transmittance and low apparent density—the latter effectuating low scattering and refractive indexes—literally invite to use these materials also for optical applications. This includes (bio)-sensing (Lim et al. 2015) and true volumetric 3D displays (Downing et al. 1996). All of these applications rely on a largely homogeneous dispersion of photoluminescent nanoparticles (*pl*-NP) within the aerogel matrix and their specific response towards

light. For sensing applications, a specific response is triggered depending on the presence and concentration of a certain target compound. Respective nanostructured porous *i*-CNF/*pl*-NP hybrid materials greatly differ from their non-porous counterparts like cellulose/*pl*-NP hybrid films (Abitbol and Gray 2008; Zeng and Yan 2015) or cellulose/*pl*-NP hybrid fibers (Kulpinski et al. 2012) in terms of properties and target applications. Preservation of scaffold nanomorphology and optical properties as well as of nanoscale size and count of accessible functional groups on the surface of the *pl*-NP for inter-particulate bonding is a major challenge along the preparation process of *i*-CNF/*pl*-NP hybrid aerogels. However, it is essential to all applications relying on both the large accessible surface of the scaffold and the nanosized scale of the functional nanoparticles.

The plethora of potential optical applications for nanostructured porous *i*-CNF/*pl*-NP hybrid materials requires selection of the most appropriate type of optical active nanoparticles. Among the wide range of *pl*-NP, carbonaceous materials are particularly appealing since they can respond to photon excitation in various ways depending on their dimensionality (Kozák et al. 2016). Beyond that, carbon dots (CDs) as one of the probably most wide-spread type of carbonaceous *pl*-NP are accessible by a multitude of both facile bottom-up and top-down syntheses approaches (Xu et al. 2016). While top-down approaches rely on laser ablation, arc discharge or

electrochemical synthesis, bottom-up strategies employ methods like thermal combustion, hydrothermal or microwave synthesis. Precursor compounds for the latter can be low-molecular organic compounds (Lim et al. 2015) or natural source materials, such as lignocellulose (Jeong et al. 2018; Rodríguez-Padrón et al. 2018), starch (Duarah and Karak 2017) or lemon juice. Carbon dots and semiconductor quantum dots have been demonstrated to share many similarities with regard to single-digit nano size or optical properties. From the perspectives of elaborateness of synthesis, health risk and environmental safety, CDs have clear advantages compared to their inorganic QD counterparts, in particular as high quantum yields of up to 80% can be reached as well (Zhu et al. 2013). Their better biocompatibility is another asset that renders them more suited for biological applications (Lim et al. 2015; Wang and Qiu 2016; Wolfbeis 2015).

Even though the principal mechanisms triggering photoluminescence in carbon dots are still a matter of debate (Lim et al. 2015; Zhu et al. 2015), it has been empirically proven that the photoluminescence properties of carbon dots including brightness and can be varied by several strategies. This includes doping of CDs with heteroelements (Xu et al. 2016), such as nitrogen (Ding et al. 2016; Xu et al. 2013, 2014; Yang et al. 2014), a combination of nitrogen and phosphor (Chandra et al. 2015) or a combination of nitrogen and sulfur (Sun et al. 2016). Variation of the size of conjugated π domains or introduction of surface functional groups carrying heteroatoms (Wolfbeis 2015) are further options in this regard.

Provided a better understanding of the mechanisms leading to photoluminescence in carbon dots, further advances in tailoring their properties for specific applications can be made. In general, the above-detailed pros of carbon dots literally invite to be used for a wide range of optical applications (Li et al. 2015; Lim et al. 2015). This includes photo-catalysis, light emitting diodes, optoelectrical devices or bio- and chemo-sensing (Yang et al. 2013). However, many of these applications require the carbon dots being dispersed and immobilized in an appropriate transparent matrix. Aerogels are ideal materials in this regard as their high interconnected porosity and large specific surface allows for loading and anchoring of larger quantities of pl-NP. Aerogels provide furthermore good accessibility of the CDs once surface-grafted by respective gaseous compounds. This can be used for

dry-state sensing (Aghajamali et al. 2016; Dolai et al. 2017; Takeshita et al. 2016; Wang et al. 2013b), such as selective detection of NO_2 (Wang et al. 2013b) and volatile organic compounds (Dolai et al. 2017) or for catalytic applications. Aerogel precursor materials, i.e. (hydro)gels (Gogoi et al. 2015; Hu et al. 2013; Sachdev et al. 2016; Wang et al. 2014) have been proposed as retrievable matrices for liquid (aqueous) applications, such as the detection and separation of heavy metal ions (Gogoi et al. 2015). Employing such matrices bears the advantage of a multiple reuse of nanoparticles at the same time inhibiting their elution into the environment.

This would be even more important for gas-phase applications which, apart from sensing, also include true volumetric 3D display applications. The latter is a vividly developing field of research which developed within short time after proof of concept, i.e. the generation of a luminescent voxel inside a transparent silica aerogel covalently equipped with upconverting semiconductor CdSe/ZnS core/shell quantum dots (Javidi et al. 2010; Sorensen et al. 2006). Recently, other matrix materials like polyvinyl alcohol (Zhu et al. 2014) or polydimethylsiloxane (Deng et al. 2015) have been successfully tested, too, partly in combination with new types of pl-NP. Among them, multicolor upconverting lanthanide-doped rare-earth metal nanoparticles (Deng et al. 2015; Zhou et al. 2015) (e.g. $NaYF_4$) are particularly promising. Excited by an appropriate setup of aligned infra-red laser beams which are first directed into a 3D laser scanner to generate the beam energy pattern specific for the 3D picture to be drawn inside the transparent matrix, both single- and multicolor $NaYF_4$ pl-NPs doted by Yb^{3+}, Nd^{3+} (sensitizers), Tm^{3+}, Ho^{3+} and Ce^{3+} ions have been demonstrated their capability of generating pictures of great color gamut (Deng et al. 2015).

Although the above hybrids are good examples for a promising symbiosis of two nanoscale materials featuring different properties, they are unlike the material we propose here: a virtually fully bio-based hybrid aerogel that combines the unique properties of a transparent nematic nanocellulosic scaffold with the photoluminescence properties of carbon dots prepared from lemon juice as a secondary renewable resource. Main emphasis of this study was to ascertain whether physical or chemical bonding of the amino-functional carbon dots onto the internal surface of the carboxylated i-CNF matrix would be the optimal way of

modification. The proviso was that the key properties of the hybrid material, such as transparency or nanomorphology should not be inferior to that of their CD-free counterparts. While physical bonding relies on electrostatic adsorption of the nanoparticles, chemical bonding employs aqueous carbodiimide coupling chemistry which already has proven efficiency in covalent bonding of CDs to nanocellulose substrates (Guo et al. 2017; Junka et al. 2014).

Materials and methods

Never-dried (50% w/w H_2O), bisulfite hardwood dissolving pulp CCOA (Potthast et al. 2003) 24.3 µmol g^{-1}, C = O, FDAM (Bohrn et al. 2006) 13.9 µmol g^{-1} COOH, Mw 303.7 kg mol^{-1}, 50% w/w) was used as cellulose starting material. Lemon juice was prepared by squeezing halved lemons using household lemon press. Filtration and subsequent centrifugation (5000 rpm, 15 min) yielded a clear extract which was stored at 4 °C until further use. 2,2,6,6-Tetramethylpiperidine-1-oxyl (TEMPO), 2,2-(ethylenedioxy)-bis-(ethylamine) (EDEA), absolute ethanol (abs. EtOH), NaBr, NaClO solution (available chlorine 10–15%), $NaClO_2$, N-(3-dimethylamino-propyl)-N′-ethylcarbodiimide hydrochloride (EDC), N-hydroxysuccinimide (NHS), quinine sulphate (QS) and 2-(N-morpholino) ethanesulfonic acid (MES) sodium salt were purchased from Sigma Aldrich (Austria) with the highest possible purity and used without further purification. Deionized water (DI H_2O, Millipore grade) was used for all procedures.

Synthesis of carbon dots (CDs)

Carbon dots were prepared by microwave-assisted co-hydrothermolysis of an organic carbon and nitrogen donor compound, similar as proposed elsewhere (Junka et al. 2014), but using lemon extract as carbon source (Hoan et al. 2018). In brief, 3 mL of 2,2-(ethylenedioxy)-bis-(ethylamine) (EDEA, nitrogen source material) was dissolved in 5 mL of lemon extract and 2 mL PBS (10 mM). The homogeneous solution was then transferred into a 100 mL round bottom flask, flushed with argon and subjected while stirring to microwave-assisted co-thermolysis at 800 W for 10 min. After cooling (30 min) the obtained dispersion of solid thermolysis products was

centrifuged at 20,000 rpm (10 min, 4° C). The supernatant was filtered through a 200 nm filter and subjected to dialysis against deionized water for 3 days using an 1 kDa membrane. The resulting dispersion of carbon dots was then lyophilized, re-dispersed in DI water to afford a concentration of 400 µg mL^{-1} (10 µg mL^{-1} for AFM) and stored at 4° C.

Atomic force microscopy

Dilute aqueous dispersions of the respective CDs and CNF were cast onto flat mica plates and dried at 105° C. Atomic force microscopy (AFM) was accomplished using a Dimension Icon Scanning Probe Microscope (Bruker AXS, Marne la Vallee, France) equipped with a NanoScope V control station. An OTESPA cantilever was used in tapping mode. NanoScope 8.15R3 software was used for the acquisition and the Gwyddion 2.47 software for image processing.

Preparation of isolated cellulose nanofibers (i-CNF) and i-CNF hydrogels

Dispersions of i-CNF were prepared by TEMPO-mediated oxidation (Isogai et al. 2011) and subsequent nanofibrillation of never-dried beech bisulfite dissolving pulp using high pressure homogenisation equipment as previously described (Plappert et al. 2018). In brief, 8 g (dry weight) of the pulp was disintegrated in 800 mL of H_2O before 128 mg 2,2,6,6-tetramethylpiperidine-1-oxyl (TEMPO), 800 mg NaBr and 12 mL NaClO solution were consecutively added. Dosage of the oxidant was accomplished at a rate of 200 µL min^{-1} and constant stirring (1000 rpm), maintaining the pH at 10 by adding of 0.1 M NaOH. After granting another 20 min reaction time, the oxidized pulp was separated by filtration and thoroughly washed with excess of deionized water. Conversion of potentially formed carbonyl to carboxyl moieties was accomplished by repeatedly (three times for 4, 6 and 15 h, respectively) treating the pre-oxidized pulp in 800 mL of 0.1 M sodium acetate buffer (pH 4.8) with 2 g of $NaClO_2$ under constant stirring (1000 rpm).

Prior to nanofibrillation, the solid content of the dispersion containing the TEMPO-oxidized cellulose was reduced to 0.5% w/w and the pH was adjusted to 8 by addition of 0.1 M NaOH. Homogenization was

performed using a high pressure laboratory homogenizer (APV 1000, APV Manufacturing Sp. z.o.o., Poland). After 5 passes at 80 MPa, the dispersion was diluted to 0.125% w/w (to prevent excessive heating caused by increasing viscosity) and 3 more passes at 80 MPa were conducted. Eventually, the obtained dispersions were centrifuged using a Rotina 380 (Hettich Lab Technology, Germany) equipped with a swing-out-rotor (1754-1778 R13) for 30 min at 5000 rpm to remove any residual agglomerates and non-fibrillated material.

The dispersions were concentrated to a solid content of 0.91 w % at which viscosity is still low enough to allow for homogeneous casting which was accomplished using cylindrical PTFE molds. The cast dispersions were submersed in 1 M HCl for 1 h to set the ordered state of self-aligned cellulose nanofibers by protonation of their surface carboxyl moieties. After removing the self-standing hydrogels from the molds, they were transferred to 50% aqueous ethanol (v/v) for setting the gel structure by lowering of the dielectric constant of the liquid while removing salt and facilitating inter-nanofiber hydrogen bonding.

Ionic and chemical bonding of carbon dots

Ionic bonding: Self-standing mixed hydro-alcogels obtained by acid-induced gelation of aqueous dispersions of 1 w % i-CNF (*cf.* above) were submersed in 1 mM HCl maintaining a solution-to-gel volumetric ratio of 5. After a residence time of 24 h the gels were transferred to a loading bath of identical HCl concentration and volume but containing additionally 0.32 mg mL^{-1} of carbon dots.

Covalent grafting of CDs was accomplished by conventional EDC/NHS carbodiimide coupling chemistry. The respective precursor gels were immersed for 24 h in five times the gel volume of 10 mM MES buffer (pH 6) before EDC and NHS were added in quantities corresponding to 25 and 100 w % of the total i-CNF content. Then the gels were transferred into a bath containing five times the gel volume of 10 mM phosphate buffer (pH 7.2) and 0.32 mg mL^{-1} of carbon dots. After a residence time of 24 h the gels of both the physical and chemical coupling approaches were left in excess of 50% aqueous ethanol for 24 h before replacing aqueous ethanol by absolute ethanol in four consecutive bathes. Both the obtained hybrid and non-modified reference alcogels were then

subjected to supercritical CO_2 drying accomplished using SF-1 supercritical fluid extraction equipment (Separex, Champigneulles, France). Extraction conditions were as follows: 9.5 MPa, 40° C, 40 g min^{-1} CO_2 flow rate, 4 h extraction time. Thereafter, the autoclave was isothermally depressurized to ambient pressure at a rate of < 0.1 MPa min^{-1}.

Samples were collected from the autoclave and stored in a desiccator until further characterization.

Light transmittance measurements

Light transmittance of both CD-free and CD-grafted i-CNF alcogels and aerogels, respectively, was studied in the wavelength range between 1100 and 300 nm using a Lambda 35 UV/VIS spectrometer (PerkinElmer, Waltham, Massachusetts, USA) and a scanning speed of 480 nm min^{-1}. The disc shaped samples had a thickness of 3.6 mm. The spectrophotometer was also used to record the absorbance of CDs at 350 nm for quantum yield determination.

Fluorescence spectroscopy

All measurements were performed on a Hitachi F-7000 fluorescence spectrophotometer (Tokyo, Japan). All measurements were carried out at 310.15 K and 700 V using a slit width of 2.5 nm for both excitation and emission spectra. Quantum yields were determined as described elsewhere (Sahu et al. 2012) using the following equation and quinine sulfate as a reference compound.

$$\Phi(x) = \Phi(st) \times \frac{m(x)}{m(st)} \times \frac{\eta^2(x)}{\eta^2(st)}$$

$\Phi(x)$: quantum yield of the target sample; $\Phi(st)$: quantum yield of QS (54%); $m(x)$, $m(st)$ are the slopes of the integrated fluorescence intensities versus absorbance which are estimated at an emission wavelength of 350 nm for 5 different concentrations. $\eta^2(x)$ and $\eta^2(st)$ are the squares of the refractive indices of the sample and the standard respectively. Respective peak areas were calculated for the quantum yield determination, using the absorbance and the integrated fluorescence intensities measured with UV/Vis spectrophotometer and fluorescence spectrophotometer respectively.

FT-IR spectroscopy

Fourier transformed infrared (FT-IR) spectra of various aerogel samples were recorded on a Perkin Elmer FTIR Spectrometer Frontier using the attenuated total reflection (ATR) mode (4000 cm^{-1} to 650 cm^{-1}, 8 scans). The spectra were normalized to their respective O-H stretching bands (at 3348 cm^{-1}).

XPS spectroscopy

XPS spectra were recorded using a Thermo Scientific instrument (K-Alpha spectrometer, Thermo Fisher Scientific, Waltham, USA) equipped with a monochromatic Al K$_\alpha$ X-ray source (1486.6 eV). High-resolution scans were performed with a pass energy of 50 eV and a step size of 0.1 eV. The peaks were fitted using a Gaussian/Lorenzian mixed function employing Shirley background correction (Software Thermo Avantage v5.957). All analyses were performed at room temperature.

Uniaxial compression of aerogels

The response of selected cellulose and cellulose-CD hybrid aerogels towards uniaxial compressive stress was recorded on a Z020 Materials Testing Machine (Zwick-Roell, Ulm, Germany) using four cylindrical specimens per variant. Strain required to achieve a deformation speed of 4.8 mm min^{-1} was measured with a 500 N load cell. Young's modulus was determined by regression from the linear portion of the stress–strain curve during reversible elastic deformation while yield point was defined at 0.2% plastic deformation.

Nitrogen sorption of aerogels

Aerogel samples were degassed in a vacuum oven at 40° C for 48 h prior to the nitrogen sorption measurements. Adsorption and desorption isotherms were recorded on a TriStar II 3020 gas sorption analyzer (Micromeritics, Norcross, USA). Specific surface areas of the samples were evaluated by applying the Brunauer–Emmett–Teller (Brunauer et al. 1938; Thommes et al. 2015) method using 11 data points of the adsorption branch of the isotherm. The area contributed by micro pores was calculated by applying the *t*-method (Lippens 1965) based on the Broekhoff–

De Boer model (Broekhoff 1968). The latter quantifies the contributions of the isotherm points correlating to a 4–6 Å thick N$_2$ layer. The nanoporous (2–100 nm) pore volume and correlating surface area contribution was evaluated with the Barrett–Joyner–Halenda (BJH) method (Barrett et al. 1951; Thommes et al. 2015). It is based on the modified Kelvin equation which also uses the Broekhoff–De Boer model (Broekhoff 1968) with the Faas correction of the desorption branch of the isotherm.

Results and discussion

Acidification of dilute aqueous dispersions of individualized cellulose I nanofibers (*i*-CNF) affords freestanding hydrogels. The latter can be converted into aerogels by consecutive solvent exchange and scCO$_2$ drying. Individualization is typically accomplished by i) TEMPO-mediated oxidation of cellulose affording 6-carboxyl cellulose and ii) subsequent mechanical nanofibrillation. Carboxylate groups formed by alkaline oxidation of accessible primary alcohol groups on the surface of cellulose fibrils—preferably in amorphous domains (Shinoda et al. 2012)—impart the final individualized nano-fibers negative surface charge. Subsequent electrostatic inter-nanofiber repulsion provides colloidal stability and balances attractive van der Waals forces (Sato et al. 2017; Wagberg et al. 2008). At concentration typically above 0.4% w/v the highly anisometric nanofibers can form anisotropic nematic structures (Kobayashi et al. 2014; Saito et al. 2011) due to entropic effects (Onsager 1949). The obtained degree of ordering can be preserved throughout acid-induced gelation and conversion into aerogels (Plappert et al. 2018). Similar materials have recently been prepared also from 2,3-dicarboxyl cellulose (2,3-DCC) (Plappert et al. 2017). Considering the requirements for matrix materials in true 3D displays, theranostic transducers or gas sensors, i.e. high transparency, full interconnectivity of voids, large specific surface and appropriate surface chemistry, *i*-CNF aerogels appear to be promising candidates in this respect.

Aiming to explore in how far the large internal surface of *i*-CNF aerogels can be homogeneously decorated with *pl*-NP and to assess the pros and cons of their covalent and ionic immobilization, respectively, cylindrical *i*-CNF hydrogels were prepared as

test matrices from 0.91 w % aqueous dispersions of individualized nanofibers. The latter were obtained by TEMPO oxidation of never-dried bisulfite hardwood dissolving pulp and subsequent nanofibrillation. The obtained *i*-CNF had an average size of 2.4 ± 0.5 nm $\times$ 940 ± 250 nm (*cf.* Fig. 1b) and a carboxyl content of 1.29 mmol g^{-1} (20.9% DO) as previously reported (Plappert et al. 2018).

Carbon dots were used as model *pl*-NP, not least because of their eco-friendliness and simple synthesis. Aiming to assess the pros and cons of chemical versus physical bonding of the CDs onto the internal surface of *i*-CNF aerogels, the carbon dots were equipped with surface amino groups which allow for both EDC/NHS-mediated covalent coupling and physical bonding through electrostatic interaction with the carboxylated *i*-CNF surfaces. The respective amino-functionalized CDs were prepared by microwave-assisted co-hydrothermolysis of 2,2-(ethylenedioxy)-bis-(ethylamine) (EDEA) and lemon juice (*cf.* Fig. 2a). While EDEA is a well-known source of nitrogen that imparts carbon dots surface amino

groups (Junka et al. 2014), lemon juice was chosen as a second precursor material since it is bio-based and consists of both carbon and nitrogen moieties due to its content of fibers, sugars and proteins. Beyond that it has recently been shown that the photoluminescence properties of lemon juice derived carbon dots can easily be controlled by varying thermolysis temperature (Hoan et al. 2018). Furthermore, carbon dots prepared from similar natural source materials were reported to feature comparatively high quantum yields (Sahu et al. 2012; Tyagi et al. 2016).

The carbon dots of this study had an average size of 1.8 ± 0.75 nm (n = 100, *cf.* Fig. 1a) as determined by atomic force microscopy and image evaluation (AFM; Fig. 1b). This is in good agreement with complementing Zetasizer particle analysis using dynamic light scattering (1.5 ± 0.6 nm; *cf.* ESI Figure 1S). UV/VIS and fluorescence spectroscopy revealed that the CDs reach their photoluminescence maximum at an excitation wavelength of $\lambda_{exc} = 251$ nm while their emission of blue light is at $\lambda_{em} = 455$ nm. The presence of surface amino groups was not explicitly studied as

Fig. 1 AFM images of carbon dots (**a**) and isolated cellulose I nanofibers obtained after TEMPO oxidation of beech sulfite pulp (**b**). Size distribution of CDs as determined by AFM image evaluation (n = 100) (**c**) and pH-dependent photoluminescence of the used CDs at $\lambda_{exc} = 340$ nm (**d**; pH steps of 7–11 are not displayed for the sake of clarity and similarity with pH 6 and 12, respectively)
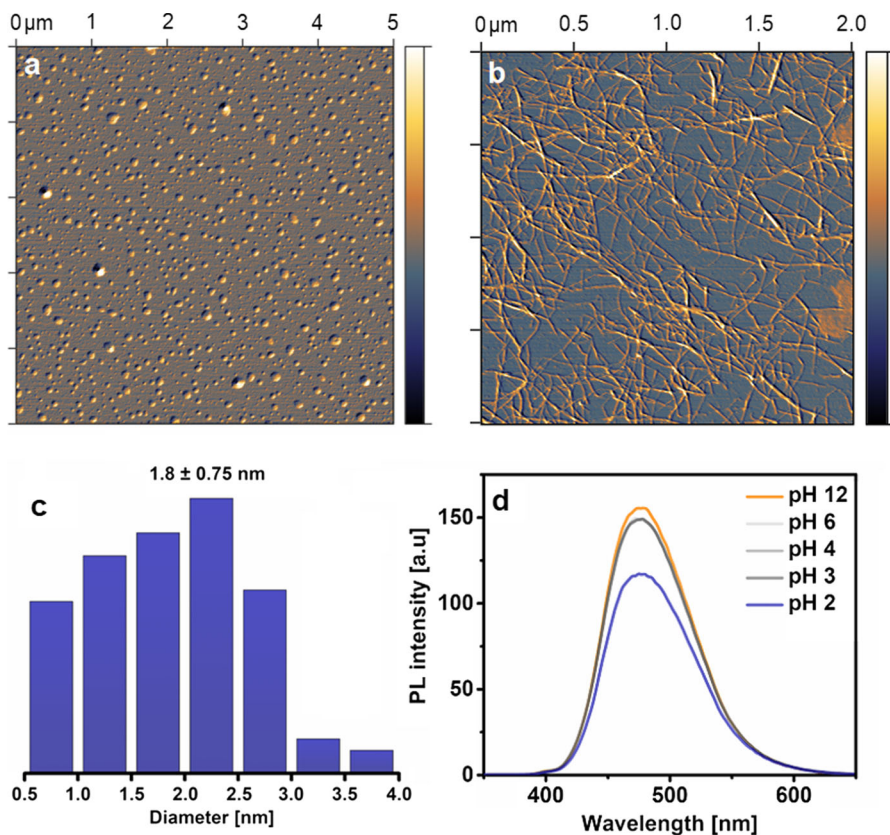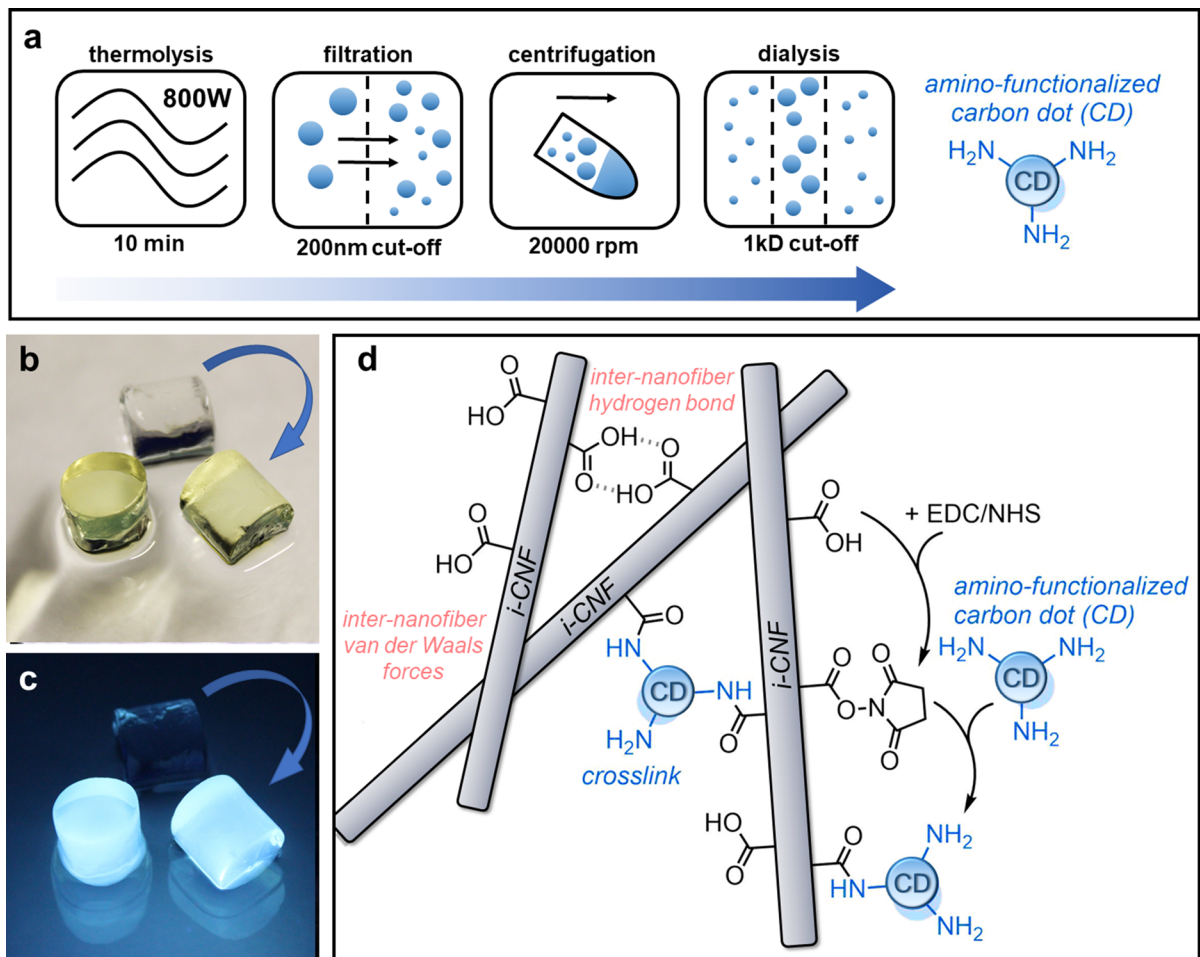
Fig. 2 Scheme of the preparation process to obtain amino-functionalized CDs (**a**). Picture of three freestanding cylindrical *i*-CNF alcogels (H: 10 mm, D: 10 mm), two chemically equipped with and one without CDs (**b**), same alcogels viewed under UV lamp 366 nm (**c**). Scheme showing inter-nanofiber bonds formed upon gel formation and the principle of EDC/NHS-mediated coupling of CDs onto the surface of *i*-CNF scaffolds after gelation (**d**)

their formation during hydrothermolysis of EDEA is well known (Junka et al. 2014). It has been also comprehensively documented in one of our previous studies (Guo et al. 2017) and was indirectly confirmed in this study by XPS spectra, FT-IR spectra (both showing amide bonds after chemical grafting), AFM pictures (CD decorated surface) and PL properties of *i*-CNF/CD hybrid aerogels after physical and chemical crosslinking (*cf.* below). As loading of the carbon dots for the two cross-linking approaches was accomplished at different pH, the photoluminescence response of respective dispersions was studied for the range of pH 2 to 12 (Fig. 1d). It turned out that at $\lambda_{\text{exc}} = 340$ nm the PL response of the CDs was largely insensitive towards pH changes however below pH 3,

a significant reduction of PL intensity was observed (Fig. 1d).

It has recently been shown that nematic *i*-CNF alcogels of comparable morphology and density can be homogeneously loaded and conformally coated with ultrathin layers of PMMA affording hybrid aerogels of greatly improved resistance towards moisture-induced shrinkage (Plappert et al. 2018).

In view of their single-digit nanometer size which is 1–2 orders of magnitude smaller than the voids of *i*-CNF aerogels, it was expected that the CDs prepared in this work would penetrate and spread across the *i*-CNF matrices with similar ease.

Both chemical and physical bonding of CDs was considered to be viable grafting strategies once the

nanoparticles were loaded, employing part of their surface amino groups as anchor sites for establishing inter-particulate cross-links to carboxyl groups on the surface of *i*-CNF. While chemical grafting was accomplished by conventional aqueous carbodiimide coupling using EDC/NHS (Fig. 2d), physical immobilization of CDs relied on pH control and electrostatic attraction between carboxylate and ammonium ions. The latter approach was particularly appealing considering its simplicity and the avoidance of any undesired side products that could be difficult to remove quantitatively from gel state. Obviously for this reason, previous studies reporting loading of bio-based matrices, such as agarose hydrogel films with chitosan-derived CDs have mostly relied on physical incorporation of the nanoparticles and not covalent bonding (Gogoi et al. 2015). Chemical grafting of CDs onto *i*-CNF in dispersion state prior gel formation was initially considered as an alternative approach. However, owing to the formation of inhomogeneous gel clusters, most likely by cross-linking of multiple *i*-CNFs through the amino-functional CDs, this approach was no longer pursued.

Acid induced gelation—based on reduction of electrostatic repulsion (Sato et al. 2017) between *i*-CNF upon protonation of surface carboxyl groups effectuated by inter-nanofiber van der Waals forces and hydrogen bonding (*cf.* Fig. 2d)—of nematic aqueous 0.9 w% *i*-CNF dispersions afforded free-standing, highly transparent hydrogels. Alcogels derived thereof by sequentially replacing water by ethanol of decreasing water content had a high light transmittance, too. It varied from 95 to 85% for a 3.6 mm thick sample in the wavelength range of 400–800 nm (*cf.* Fig. 5). Volumetric shrinkage in the sum of acid-induced gelation and the solvent exchange steps was 4–5% only for the reference, carbon dot free alcogels.

Loading of the amino functional carbon dots according to the protocol for physical grafting, i.e. in protonated state at pH 4, and the subsequent washing and solvent exchange steps increasing the pH to about 6–7 did not translate into enhanced shrinkage. This was different for the chemical EDC/NHS crosslinking approach as the alcogels suffered from an additional volumetric shrinkage of up to 20%, probably due to formation of more rigid networks of reduced specific volume.

The extent of shrinkage during scCO$_2$ drying was the same for all gels (Table 1). Correspondingly, higher CD densities were obtained for both alcogels and aerogels of the covalent bonding approach due to the contraction of the respective alcogels during loading and chemical grafting of the CDs. This is evident from the faint yellow color of the obtained materials (*cf.* Fig. 4e, right) and their stronger adsorption of light in the lower wavelength range of the visible light (300–500 nm; Fig. 3a). It is also confirmed by photoluminescence spectra ($\lambda_{exc} = 350$ nm) which show higher PL intensities for the alcogels (fourfold) and aerogels (tenfold) containing covalently immobilized carbon dots (Fig. 3b).

However, considering their similar volumetric contraction upon scCO$_2$ drying, the over-proportional increase of Δ PL$_{max}$ (PL$_{max, chem}$/PL$_{max, phys}$) for the aerogels of the two coupling approaches clearly suggests that part of the CDs is lost by extraction with the supercritical fluid.

A minor decrease in PL intensity has been also observed during scCO$_2$ drying of the gels of the covalent grafting approach (Figs. 3b, 4g, h). However, this effect is known to be caused by scattering losses in the resulting aerogels and has been reported for cellulose aerogels covalently equipped with semiconductor quantum dots, too (Wang et al. 2013a). The stronger scattering, in particular at lower wavelengths, is attributed to Rayleigh scattering which occurs due to

Table 1 Composition, shrinkage and apparent density of CNF alcogels physically and chemically equipped with CDs

	Initial CNF content (w%)	Shrinkage caused by coupling (v%)	Shrinkage caused by drying (v%)	Bulk density (mg cm^{-3})
Reference	0.91	0	35	15.4
Physical	0.91	0	37	16.3
Chemical	0.91	20	35	20.1

Fig. 3 Light transmission (**a**) and photoluminescence spectra (**b**, λ_exc = 350 nm) of *i*-CNF/CD-chem versus *i*-CNF/CD-phys hybrid alcogels (3.6 mm thickness) and aerogels, respectively, as well as of their CD-free counterparts
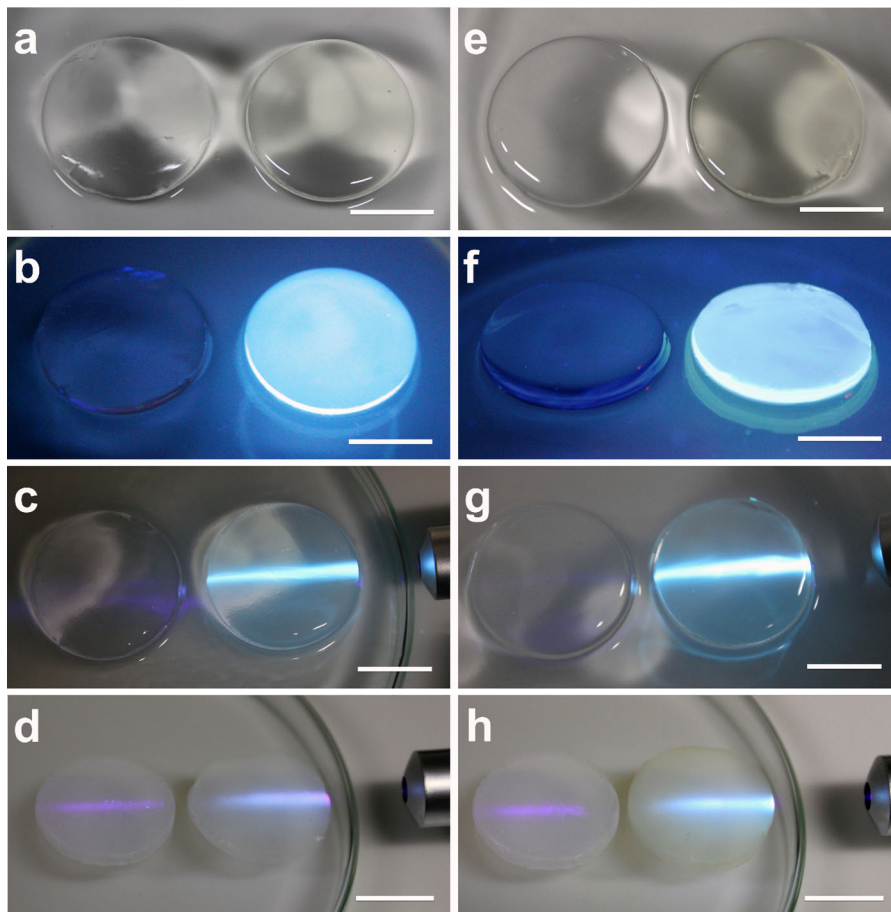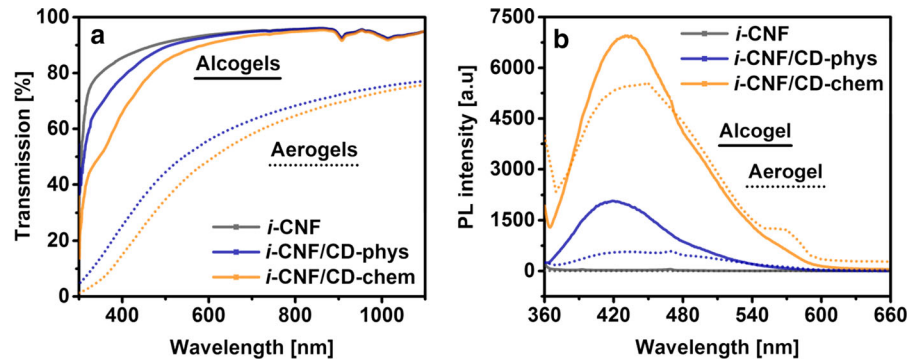

Fig. 4 CNF alcogels (**a–c**, **e–g**) and aerogels (**d**, **h**) without CDs (left in each picture) and with coupled CDs (right in each picture); physically coupled (**a–c**); chemically coupled (**e–g**); **a**, **e** under normal light, **b**, **f** under UV lamp 366 nm, **c**, **d**, **g**, **h** under normal light with a laser beam (405 nm, 100 mW) crossing through both gels (from the right). Note: the scale bar corresponds to 1 cm

the lower refraction index of air (compared to ethanol in case of alcogels) filling the interconnected void system of the aerogels and the resulting higher refraction at the multiple phase boundaries between voids and solid network structure. The scattering effects can be nicely visualized by illuminating both CD-free and CD-containing samples with a 405 nm laser beam (*cf.* Fig. 4d, h). While scattering of the laser

Fig. 5 FT-IR (**a**, section) and XPS spectra **b** of *i*-CNF aerogels whose internal surface was decorated with amino-functional carbon dots either by chemical or physical bonding
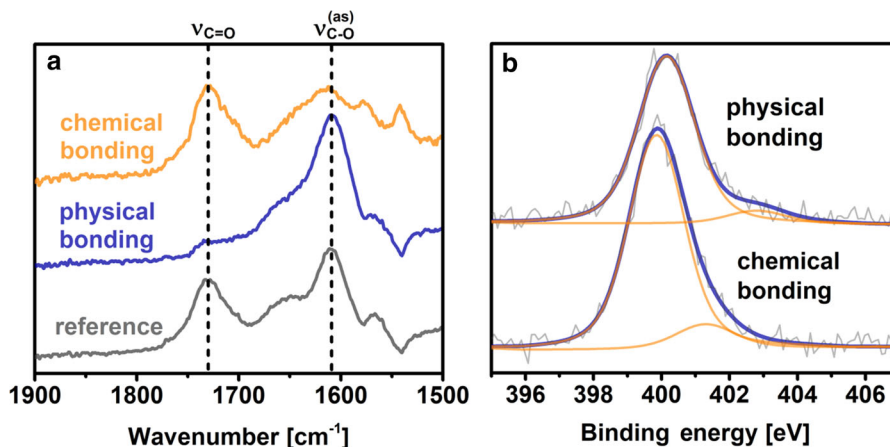
beam can be nicely seen in the CD-free reference aerogels (left samples in Fig. 4d, h), it is almost not visible in the respective alcogels (left sample Fig. 4c, g).

Besides from the strong photoluminescence of both *i*-CNF/CD hybrid alcogels and aerogels matching the PL properties of the implemented carbon dots (Fig. 4), the successful decoration of the internal surface of the *i*-CNF aerogels is also evident from FT-IR and X-ray photoelectron spectroscopy (XPS) analyses (Fig. 5).

The FT-IR spectra obtained are comparable with that of a recent study investigating improvement of the thermal stability of TEMPO-oxidized cellulose nanofibers by coupling with amine-terminated polyethylene glycol and employing heat-induced conversion of initially formed ionic bonds into amide bonds (Lavoine et al. 2016). Evaluation of the FT-IR spectral region between 1800 cm^{-1} and 1500 cm^{-1} provided valuable information on the bonding state of (C6) carboxyl moieties of TEMPO-oxidized cellulose (Fukuzumi et al. 2013; Lavoine et al. 2016). While the band around 1610 cm^{-1} represent asymmetric (as) stretching of C–O bonds, stretching of C=O bonds is visible at 1730 cm^{-1} (Fig. 5a). Aerogels containing no CDs show signals for both C–O and C=O bonds as expected for protonated carboxyl moieties. Spectra of aerogels containing physically coupled CDs on the other hand virtually lack the C=O bands due to the resonance structure of the carboxylate anion formed by proton transfer to the amino-CDs. The contrary is the case for chemically modified aerogels which show only a very week C–O signal due to the formation of amide bonds while the C=O bonds is still present (Fig. 5a).

XPS spectra of the two types of *i*-CNF/CD hybrid aerogels confirm the existence of the respective interparticulate bonding moieties between surface carboxyl(ate) groups of the cellulosic nanofibers and surface amino groups of the carbon dots. Besides the dominating peak at around 400 eV binding energy (E_B) which is caused by the abundance of amino groups on the surface of the carbon dots (Guo et al. 2017; Oh et al. 2013) two smaller peaks at higher binding energies appear in the N 1 s spectra. Based on literature values (Beamson and Briggs 1992; Oh et al. 2013) and following the rule that increasing acidity of the nitrogen atom shifts E_B towards higher values (Beamson and Briggs 1992), the small peaks at 401.2 eV and 402.9 eV were assigned to secondary amide and quaternary ammonium moieties, respectively.

Investigation of the mechanical response of the different types of hybrid aerogels towards compressive stress revealed that both stiffness and strength as expressed by the parameters Young's modulus (*E*) and offset yield stress $\sigma_{0.2\%}$ only slightly increased compared to the CD-free reference aerogels (Table 2). However, normalization of *E* for bulk density (specific modulus E_ρ) suggests somewhat higher stiffness for this type of hybrid aerogel. The Young's modulus of the materials obtained by chemical bonding of CDs was almost more than twice as high as for the reference aerogels. While this effect is owed partly to the somewhat higher density of these hybrid aerogels, it is evident that other factors contribute as well. The recorded stress–strain-curves (*cf.* Fig. 6) reveal that the yield point is also almost twice as high compared to *i*-CNF/CD hybrid aerogels of the physical bonding

Table 2 Physical, mechanical and morphological properties of *i*-CNF and *i*-CNF/CD hybrid aerogels containing either physically or chemically bonded carbon dots on their internal surface

	Bulk density (mg cm^{-3})	Yield stress (0.2% PD[a])[b] (KPa)	Young's modulus[b] (KPa)	Specific modulus[b] (GPa m^3 kg^{-1})	Specific surface (m^{2}g^{-1})	Micropore area (t-plot) (m^2 g^{-1})
Reference	15.4	15.2 ± 1.7	263.6 ± 39.7	17.1	317	47
Physical	16.3	15.8 ± 1.5	346.7 ± 47.0	21.3	345	56
Chemical	20.1	31.0 ± 6.7	470.0 ± 113.1	23.4	491	64

[a]Plastic deformation

[b]n = 4
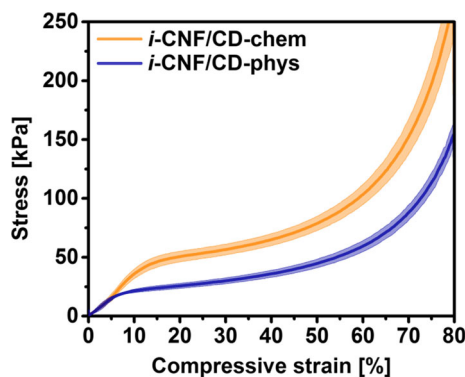
Fig. 6 Physical versus chemical grafting of carbon dots—mechanical response of *i*-CNF/CD hybrid aerogels towards uniaxial compression stress (4.8 mm min^{-1}). A respective reference stress–strain curve for an unmodified *i*-CNF aerogel of comparable density can be found elsewhere (Plappert et al. 2018; Table 2)

approach. Therefore, it is safe to conclude that covalent crosslinking (*cf.* Fig. 2d) significantly increases the strength of respective *i*-CNF/CD hybrid aerogels. Simultaneously, they are more elastic than the materials of the physical bonding approach and exhibit, hence, higher resilience.

Nitrogen sorption experiments at 77 K and evaluation of the sorption isotherms (11 data points of the adsorption branch) for the Brunauer–Emmett–Teller (BET) surface area revealed that covalent immobilization of carbon dots affords hybrid aerogels of significantly higher internal surface (491 m^2 g^{-1}, 9.87 m^2 cm^{-3}) compared to the physical bonding approach (345 m^2 g^{-1}, 5.62 m^2 cm^{-3}). The CD-free reference material had the lowest specific surface (317 m^2 g^{-1}, 4.88 m^2 cm^{-3}).

The conducted nitrogen sorption experiments also confirmed that *i*-CNF aerogels and *i*-CNF/CD hybrid aerogels feature a largely interconnected, multi-scale porosity comprising micro-, meso- and macro pores (*cf.* FEG-SEM image, ESI Figure S3). The IUPAC type IV (Thommes et al. 2015) shape of the isotherms (*cf.* ESI Figure S2,) and the Barrett–Joyner–Halenda (BJH) pore size distribution plots (Fig. 7a), however, clearly show that for all materials the majority of surface area is contributed by mesopores while the contribution of micro-(Table 2) and macropores (Fig. 7b) is much lower. Even though gas sorption experiments do not allow for a comprehensive characterization of the full macropore scale, their results can be used to reveal differences between the materials of the two coupling approaches related to their micro- and mesopore fractions as well as those small macropores whose diameters do not exceed about 100 nm.

Analysis of the sorption isotherms using the BJH model showed that all studied materials including the CD-free reference aerogels had a largely similar pore size distribution peaking at around 50 nm and suggesting that the different coupling approaches had no significant impact onto the nanomorphology of the CNF scaffolds. This is plausible considering that the cellulose nanofibers have assembled into a free-standing relatively rigid network already at the hydrogel state before the CDs are loaded and grafted onto their surface. However, compared to the *i*-CNF/CD-phys hybrid aerogels it is evident that the materials of the covalent bonding approach have more pores below 10 nm contributing to their higher pore volume and specific surface area (Fig. 7b).

The slope (and intercept) of the t-plot derived by applying the de-Boer equation to multilayer nitrogen adsorption data outside the micropore range indicate

Fig. 7 Pore size distribution relating to pore area (**a**) and pore volume (**b**) of CD-free aerogels (*i*-CNF) as well as *i*-CNF/CD-phys and *i*-CNF/CD-chem hybrid aerogels
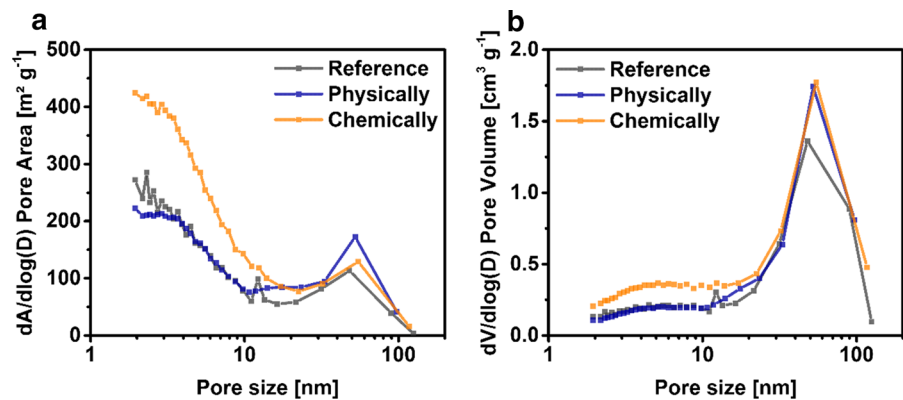
that the count of micropores and, hence, micropore area increases with the introduction of carbon dots (*cf.* Table 2). This is most pronounced for *i*-CNF/CD-chem hybrid aerogels while physical immobilization of CDs had a minor effect only. It is assumed that the overall increase of specific surface area (S_{BET}) with a main contribution of small mesopores (2–10 nm) is directly proportional to both count and accessible surface area of the carbon dots introduced by the respective coupling approaches. The considerable difference in S_{BET} gain related to the CD-free reference material (*i*-CNF/CD-chem: 175 m^2 g^{-1}; *i*-CNF/CD-phys: 30 m^2 g^{-1}; *cf.* Table 2) roughly correlates with the difference in photoluminescent response of the two types of hybrid aerogels and emphasizes the superiority of the chemical bonding approach. From an application perspective, this study has been demonstrated that loading of amino-functional *pl*-NP and their covalent immobilization on the large internal surface of carboxyl-functional *i*-CNF gels can afford aerogels that combine all of the characteristics needed to account for a promising bio-based matrix material for gas sensing or true volumetric displays. They are transparent, lightweight, have high interconnected porosity and, hence, high accessibility of the introduced CDs (Plappert et al. 2018; Kobayashi et al. 2014). Optionally, respective cellulose hybrid aerogels can be conformally coated by secondary biocompatible polymers, such as PMMA to render them insensitive towards moisture induced shrinkage (Plappert et al. 2018).

Conclusions

This study has demonstrated that loading of *pl*-NP, specifically of amino-functional carbon dots, from dispersion state into the virtually fully interconnected void system of nematically ordered and largely mesoporous gel matrix composed of self-aligned cellulose I nanofibers (*i*-CNF; Plappert et al. 2018) and their subsequent physical or chemical bonding to surface carboxyl groups affords homogeneous nematic nanocomposite hydrogels. The latter can be converted into aerogels by consecutive solvent exchange and scCO$_2$ drying. Since the high light transmittance and nanomorphology of *i*-CNF alcogels is virtually not compromised by incorporation of *pl*-NP under the tested conditions, it is safe to conclude that the investigated approaches hold some promises with regard to the development of optical devices. While optical sensors rely on a sufficient density of reporter nanoparticles dispersed across a large internal surface which is fully accessible to soluble (lyogels) or gaseous (aerogels) target analytes, true volumetric 3D displays require low scattering and highly transparent matrix materials. In case of volumetric displays, the homogeneously distributed *pl*-NP should be topologically fixed and feature upconverting properties. This is required for an appropriate setup of IR lasers, dichroic mirror and 3D laser scanner to generate high resolution color pictures within a respective 3D matrix. Not least because of this aspect, covalent immobilization of the nanoparticles represents the superior approach as evident from the serious leaching issue with physical *pl*-NP bonding, loss of PL intensity and inferior internal surface and mechanical properties.

Author contributions SQ and SFP share the first authorship of this manuscript since both contributed equally. SQ prepared and characterized carbon dots, performed and designed all fluorescence measurements and contributed a significant part of the writing of the initial manuscript. SFP designed the coupling and loading procedures, prepared the cellulose gels (and aerogels) and conducted and designed mechanical characterization, gas sorption experiments, some of the UV–Vis measurements, designed figures and contributed a significant part of the writing of the manuscript. FWL conceived the idea of the project, acquired funding, provided project management, supervised and developed the individual tasks, and contributed comprehensive revision of the initial manuscript. TG contributed XPS analysis and evaluation. WG-A helped significantly with planning, conducting and evaluation of AFM and mechanical analyses.

Compliance with ethical standards

Conflict of interest The author declares that they have no conflict of interest.

References

Abitbol T, Gray DG (2008) Incorporation into paper of cellulose triacetate films containing semiconductor nanoparticles. Cellulose 16:319–326. https://doi.org/10.1007/s10570-008-9263-z

Aghajamali M, Iqbal M, Purkait TK, Hadidi L, Sinelnikov R, Veinot JGC (2016) Synthesis and properties of luminescent silicon nanocrystal/silica aerogel hybrid materials. Chem Mater 28:3877–3886. https://doi.org/10.1021/acs.chemmater.6b01114

Barrett EP, Joyner LG, Halenda PP (1951) The determination of pore volume and area distributions in porous substances. I Computations from nitrogen isotherms. J Am Chem Soc 73:373–380. https://doi.org/10.1021/ja01145a126

Beamson G, Briggs D (1992) High resolution XPS of organic polymers: the scienta ESCA300 database. Wiley, Chichester

Bohrn R, Potthast A, Schiehser S, Rosenau T, Sixta H, Kosma P (2006) The FDAM method: determination of carboxyl profiles in cellulosic materials by combining group-selective fluorescence labeling with GPC. Biomacromolecules 7:1743–1750. https://doi.org/10.1021/bm060039h

Broekhoff J (1968) Studies on pore systems in catalysts XIII. Pore distributions from the desorption branch of a nitrogen sorption isotherm in the case of cylindrical pores B. Appl J Catal 10:377–390. https://doi.org/10.1016/0021-9517(68)90153-x

Brunauer S, Emmett PH, Teller E (1938) Adsorption of gases in multimolecular layers. J Am Chem Soc 60:309–319. https://doi.org/10.1021/ja01269a023

Chandra S, Laha D, Pramanik A, Ray Chowdhuri A, Karmakar P, Sahu SK (2015) Synthesis of highly fluorescent nitrogen and phosphorus doped carbon dots for the detection of Fe ions in cancer cells. Luminescence. https://doi.org/10.1002/bio.2927

Deng R, Qin F, Chen R, Huang W, Hong M, Liu X (2015) Temporal full-colour tuning through non-steady-state upconversion. Nat Nanotechnol 10:237–242. https://doi.org/10.1038/nnano.2014.317

Ding H, Yu SB, Wei JS, Xiong HM (2016) Full-color light-emitting carbon dots with a surface-state-controlled luminescence mechanism. ACS Nano 10:484–491. https://doi.org/10.1021/acsnano.5b05406

Dolai S, Bhunia SK, Jelinek R (2017) Carbon-dot-aerogel sensor for aromatic volatile organic compounds. Sens Actuators B 241:607–613. https://doi.org/10.1016/j.snb.2016.10.124

Downing E, Hesselink L, Ralston J, Macfarlane R (1996) A three-color, solid-state, three-dimensional display. Science 273:1185–1189. https://doi.org/10.1126/science.273.5279.1185

Duarah R, Karak N (2017) Facile and ultrafast green approach to synthesize biobased luminescent reduced carbon nanodot: an efficient photocatalyst. ACS Sustain Chem Eng 5:9454–9466. https://doi.org/10.1021/acssuschemeng.7b02590

Fukuzumi H, Fujisawa S, Saito T, Isogai A (2013) Selective permeation of hydrogen gas using cellulose nanofibril film. Biomacromolecules 14:1705–1709. https://doi.org/10.1021/bm400377e

Gogoi N, Barooah M, Majumdar G, Chowdhury D (2015) Carbon dots rooted agarose hydrogel hybrid platform for optical detection and separation of heavy metal ions. ACS Appl Mater Interfaces 7:3058–3067. https://doi.org/10.1021/am506558d

Guo J et al (2017) Photoluminescent hybrids of cellulose nanocrystals and carbon quantum dots as cytocompatible probes for in vitro bioimaging. Biomacromolecules 18:2045–2055. https://doi.org/10.1021/acs.biomac.7b00306

Hoan BT, Van Huan P, Van HN, Nguyen DH, Tam PD, Nguyen KT, Pham VH (2018) Luminescence of lemon-derived carbon quantum dot and its potential application in luminescent probe for detection of Mo(6+) ions. Luminescence 33:545–551. https://doi.org/10.1002/bio.3444

Hu S, Zhao Q, Dong Y, Yang J, Liu J, Chang Q (2013) Carbon-dot-loaded alginate gels as recoverable probes: fabrication and mechanism of fluorescent detection. Langmuir 29:12615–12621. https://doi.org/10.1021/la402647t

Isogai A, Saito T, Fukuzumi H (2011) TEMPO-oxidized cellulose nanofibers Nanoscale 3:71–85. https://doi.org/10.1039/c0nr00583e

Javidi B, Marinov VR, Lima JIT, Miller R, Son J-Y, Thomas JT, Desjardins DD (2010) Quantum dot dispersions in aerogels: a new material for true volumetric color displays. Proc SPIE 7690:76900X–76900X–76907. https://doi.org/10.1117/12.850252

Jeong Y, Moon K, Jeong S, Koh W-G, Lee K (2018) Converting waste papers to fluorescent carbon dots in the recycling process without loss of ionic liquids and bioimaging applications. ACS Sustain Chem Eng 6:4510–4515. https://doi.org/10.1021/acssuschemeng.8b00353

Jiang F, Hsieh Y-L (2016) Self-assembling of TEMPO oxidized cellulose nanofibrils as affected by protonation of surface carboxyls and drying methods. ACS Sustain Chem Eng 4:1041–1049. https://doi.org/10.1021/acssuschemeng.5b01123

Junka K, Guo J, Filpponen I, Laine J, Rojas OJ (2014) Modification of cellulose nanofibrils with luminescent carbon dots. Biomacromolecules 15:876–881. https://doi.org/10.1021/bm4017176

Kobayashi Y, Saito T, Isogai A (2014) Aerogels with 3D ordered nanofiber skeletons of liquid-crystalline nanocellulose derivatives as tough and transparent insulators. Angew Chem Int Ed Engl 53:10394–10397. https://doi.org/10.1002/anie.201405123

Korhonen JT, Hiekkataipale P, Malm J, Karppinen M, Ikkala O, Ras RH (2011) Inorganic hollow nanotube aerogels by atomic layer deposition onto native nanocellulose templates. ACS Nano 5:1967–1974. https://doi.org/10.1021/nn200108s

Kozák O, Sudolská M, Pramanik G, Cígler P, Otyepka M, Zbořil R (2016) Photoluminescent carbon nanostructures. Chem Mater 28:4085–4128. https://doi.org/10.1021/acs.chemmater.6b01372

Kulpinski P, Erdman A, Namyslak M, Fidelus JD (2012) Cellulose fibers modified by Eu3+-doped yttria-stabilized zirconia nanoparticles. Cellulose 19:1259–1269. https://doi.org/10.1007/s10570-012-9704-6

Lavoine N, Bras J, Saito T, Isogai A (2016) Improvement of the thermal stability of TEMPO-oxidized cellulose nanofibrils by heat-induced conversion of ionic bonds to amide bonds. Macromol Rapid Commun 37:1033–1039

Li S, Huang J (2016) Cellulose-rich nanofiber-based functional nanoarchitectures. Adv Mater 28:1143–1158. https://doi.org/10.1002/adma.201501878

Li X, Rui M, Song J, Shen Z, Zeng H (2015) Carbon and graphene quantum dots for optoelectronic and energy devices: a review. Adv Funct Mater 25:4929–4947. https://doi.org/10.1002/adfm.201501250

Lim SY, Shen W, Gao Z (2015) Carbon quantum dots and their applications. Chem Soc Rev 44:362–381. https://doi.org/10.1039/c4cs00269e

Lippens B (1965) Studies on pore systems in catalysts V. The t method. J Catal 4:319–323. https://doi.org/10.1016/0021-9517(65)90307-6

Oh D, Shin S, Lim C, Hwang D (2013) Dopamine-mediated sclerotization of regenerated chitin in ionic liquid. Materials 6:3826–3839

Olsson RT et al (2010) Making flexible magnetic aerogels and stiff magnetic nanopaper using cellulose nanofibrils as templates. Nat Nanotechnol 5:584–588. https://doi.org/10.1038/nnano.2010.155

Onsager L (1949) The effects of shape on the interaction of colloidal particles. Ann N Y Acad Sci 51:627–659. https://doi.org/10.1111/j.1749-6632.1949.tb27296.x

Plappert SF, Nedelec J-M, Rennhofer H, Lichtenegger HC, Liebner FW (2017) Strain hardening and pore size harmonization by uniaxial densification: a facile approach toward superinsulating aerogels from nematic nanofibrillated 2,3-dicarboxyl cellulose. Chem Mater 29:6630–6641. https://doi.org/10.1021/acs.chemmater.7b00787

Plappert SF, Quraishi S, Nedelec J-M, Konnerth J, Rennhofer H, Lichtenegger HC, Liebner FW (2018) Conformal ultrathin coating by scCO$_2$-mediated PMMA deposition: a facile approach to add moisture resistance to lightweight ordered nanocellulose aerogels. Chem Mater 30:2322–2330

Potthast A, Rohrling J, Rosenau T, Borgards A, Sixta H, Kosma P (2003) A novel method for the determination of carbonyl groups in cellulosics by fluorescence labeling. 3. Monitoring oxidative processes. Biomacromolecules 4:743–749. https://doi.org/10.1021/bm025759c

Rodríguez-Padrón D et al (2018) Catalyzed microwave-assisted preparation of carbon quantum dots from lignocellulosic residues. ACS Sustain Chem Eng 6:7200–7205. https://doi.org/10.1021/acssuschemeng.7b03848

Sachdev A, Matai I, Gopinath P (2016) Carbon dots incorporated polymeric hydrogels as multifunctional platform for imaging and induction of apoptosis in lung cancer cells. Colloids Surf B 141:242–252. https://doi.org/10.1016/j.colsurfb.2016.01.043

Sahu S, Behera B, Maiti TK, Mohapatra S (2012) Simple one-step synthesis of highly luminescent carbon dots from orange juice: application as excellent bio-imaging agents. Chem Commun (Camb) 48:8835–8837. https://doi.org/10.1039/c2cc33796g

Saito T, Uematsu T, Kimura S, Enomae T, Isogai A (2011) Self-aligned integration of native cellulose nanofibrils towards producing diverse bulk materials. Soft Matter 7:8804. https://doi.org/10.1039/c1sm06050c

Sato Y, Kusaka Y, Kobayashi M (2017) Charging and aggregation behavior of cellulose nanofibers in aqueous solution. Langmuir 33:12660–12669. https://doi.org/10.1021/acs.langmuir.7b02742

Shinoda R, Saito T, Okita Y, Isogai A (2012) Relationship between length and degree of polymerization of TEMPO-oxidized cellulose nanofibrils. Biomacromolecules 13:842–849. https://doi.org/10.1021/bm2017542

Sorensen L, Strouse G, Stiegman A (2006) Fabrication of stable low-density silica aerogels containing luminescent ZnS capped CdSe quantum dots. Adv Mater 18:1965

Sun C et al (2016) Synthesis of nitrogen and sulfur co-doped carbon dots from garlic for selective detection of Fe(3). Nanoscale Res Lett 11:110. https://doi.org/10.1186/s11671-016-1326-8

Takeshita S, Takebayashi Y, Nakamura H, Yoda S (2016) Gas-responsive photoluminescence of YVO4:Eu3+

nanoparticles dispersed in an ultralight, three-dimensional nanofiber network. Chem Mater 28:8466–8469. https://doi.org/10.1021/acs.chemmater.6b04160

Thommes M, Kaneko K, Neimark AV, Olivier JP, Rodriguez-Reinoso F, Rouquerol J, Sing KSW (2015) Physisorption of gases, with special reference to the evaluation of surface area and pore size distribution (IUPAC Technical Report). Pure Appl Chem 87:1051. https://doi.org/10.1515/pac-2014-1117

Toivonen MS, Kaskela A, Rojas OJ, Kauppinen EI, Ikkala O (2015) Ambient-dried cellulose nanofibril aerogel membranes with high tensile strength and their use for aerosol collection and templates for transparent, flexible devices. Adv Funct Mater 25:6618–6626. https://doi.org/10.1002/adfm.201502566

Tyagi A, Tripathi KM, Singh N, Choudhary S, Gupta RK (2016) Green synthesis of carbon quantum dots from lemon peel waste: applications in sensing and photocatalysis. RSC Adv 6:72423–72432. https://doi.org/10.1039/c6ra10488f

Wagberg L, Decher G, Norgren M, Lindstrom T, Ankerfors M, Axnas K (2008) The build-up of polyelectrolyte multilayers of microfibrillated cellulose and cationic polyelectrolytes. Langmuir 24:784–795. https://doi.org/10.1021/la702481v

Wang J, Qiu J (2016) A review of carbon dots in biological applications. J Mater Sci 51:4728–4738. https://doi.org/10.1007/s10853-016-9797-7

Wang H, Shao Z, Bacher M, Liebner F, Rosenau T (2013a) Fluorescent cellulose aerogels containing covalently immobilized (ZnS)x(CuInS2)1 − x/ZnS (core/shell) quantum dots. Cellulose. https://doi.org/10.1007/s10570-013-0035-z

Wang R, Li G, Dong Y, Chi Y, Chen G (2013b) Carbon quantum dot-functionalized aerogels for NO$_2$ gas sensing. Anal Chem 85:8065–8069. https://doi.org/10.1021/ac401880h

Wang F, Xie Z, Zhang B, Liu Y, Yang W, Liu CY (2014) Down- and up-conversion luminescent carbon dot fluid: inkjet printing and gel glass fabrication. Nanoscale 6:3818–3823. https://doi.org/10.1039/c3nr05869g

Wolfbeis OS (2015) An overview of nanoparticles commonly used in fluorescent bioimaging. Chem Soc Rev 44:4743–4768. https://doi.org/10.1039/c4cs00392f

Xu Y, Wu M, Liu Y, Feng XZ, Yin XB, He XW, Zhang YK (2013) Nitrogen-doped carbon dots: a facile and general preparation method, photoluminescence investigation, and imaging applications. Chemistry 19:2276–2283. https://doi.org/10.1002/chem.201203641

Xu M et al (2014) A green heterogeneous synthesis of N-doped carbon dots and their photoluminescence applications in solid and aqueous states. Nanoscale 6:10307–10315. https://doi.org/10.1039/c4nr02792b

Xu Q et al (2016) Heteroatom-doped carbon dots: synthesis, characterization, properties, photoluminescence mechanism and biological applications. J Mater Chem B 4:7204–7219. https://doi.org/10.1039/c6tb02131j

Yang Z et al (2013) Controllable synthesis of fluorescent carbon dots and their detection application as nanoprobes. Nano Micro Lett 5:247–259. https://doi.org/10.1007/bf03353756

Yang Z et al (2014) Nitrogen-doped, carbon-rich, highly photoluminescent carbon dots from ammonium citrate. Nanoscale 6:1890–1895. https://doi.org/10.1039/c3nr05380f

Zeng J, Yan L (2015) Metal-free transparent luminescent cellulose films. Cellulose 22:729–736. https://doi.org/10.1007/s10570-014-0485-y

Zhou B, Shi B, Jin D, Liu X (2015) Controlling upconversion nanocrystals for emerging applications. Nat Nanotechnol 10:924–936. https://doi.org/10.1038/nnano.2015.251

Zhu S et al (2013) Highly photoluminescent carbon dots for multicolor patterning, sensors, and bioimaging. Angew Chem Int Ed Engl 52:3953–3957. https://doi.org/10.1002/anie.201300519

Zhu M, Zhong H, Jia J, Fu W, Liu J, Zou B, Wang Y (2014) PVA hydrogel embedded with quantum dots: a potential scalable and healable display medium for holographic 3D applications. Adv Opt Mater 2:338–342. https://doi.org/10.1002/adom.201300517

Zhu S, Song Y, Zhao X, Shao J, Zhang J, Yang B (2015) The photoluminescence mechanism in carbon dots (graphene quantum dots, carbon nanodots, and polymer dots): current state and future perspective. Nano Res 8:355–381. https://doi.org/10.1007/s12274-014-0644-3

Zhu L, Zong L, Wu X, Li M, Wang H, You J, Li C (2018) Shapeable fibrous aerogels of metal-organic-frameworks templated with nanocellulose for rapid and large-capacity adsorption. ACS Nano 12:4462–4468. https://doi.org/10.1021/acsnano.8b00566